SUPPLEMENTAL MATERIAL

Unmasking Arrhythmogenic hubs of reentry driving persistent atrial fibrillation for patient-specific treatment

Hansen et al: Unmasking atrial fibrillation drivers

Authors:

Brian J Hansen, PhD[a,b]; Jichao Zhao, PhD[c]; Katelynn M Helfrich, BSc[a,b]; Ning Li, MD, PhD[a,b]; Alexander Iancau[a]; Alexander Zolotarev, MD[a,d]; Stanislav O Zakharkin, PhD[a]; Anuradha Kalyanasundaram, PhD[a,b]; Megan Subr [a]; Nawshin Dastagir PhD[c]; Roshan Sharma, BSc[c] ; Esthela Artiga, MSc[a,b]; Nicholas Salgia, BSc[a]; Mustafa M Houmsse[a]; Omar Kahaly, MD[b,e], Paul ML Janssen, PhD[a,b]; Peter J Mohler, PhD[a,b]; Nahush A Mokadam, MD[b,f]; Bryan Whitson, MD, PhD[b,f]; Muhammad R Afzal, MD[b,e]; Orlando P Simonetti, PhD[b,g]; John D Hummel, MD[b,e*]; Vadim V Fedorov, PhD[a,b*]

Affiliations: aDepartment of Physiology & Cell Biology and Frick Center for Heart Failure and Arrhythmia; bDavis Heart & Lung Research Institute The Ohio State University Wexner Medical Center, Columbus, OH, USA; cUniversity of Auckland, Auckland, New Zealand; dSkolkovo Institute of Science and Technology, Moscow, Russia; eDepartment of Internal Medicine; fDivision of Cardiac Surgery; gDepartment of Biomedical Engineering, The Ohio State University Wexner Medical Center, Columbus, OH

EXPANDED MATERIALS AND METHODS

Study design

The objective of this study was to explore the utility of modulating atrial fibrillation (AF) driver physiology, specifically atrial refractoriness, to increase driver stability and subsequent identification by multi-electrode mapping (MEM) for targeted ablation treatment. Due to great variation between species[46], observations of AF drivers made from animal models may not be directly applicable to the human heart. Furthermore, existing clinical surface-electrode recordings[2, 4, 8, 47] are unable to provide definitive data on AF drivers located intramurally within the atrium. Thus, we developed a novel integrated approach to study the functional and structural features of the explanted human heart under controlled laboratory experiments. These findings were then translated to a study in a limited number of persistent AF patients as a pilot clinical study to assess the utility of adenosine bolus to improve AF driver detection with MEM for targeted ablation treatment (**Figure S1**). *Ex-vivo* sample sizes were chosen based on power calculations after previous *ex-vivo* human studies[6, 11, 13] to estimate population mean and standard deviation (SD). The number of patients considered for the study was based first on our initial *ex-vivo* human heart studies[13] and then the expected incidence rate of acute AF termination during ablation procedures.[42]

Ex-Vivo Functionally and 3D Structurally Mapped Human Atria and Subsequent Image-based Heart-Specific 3D Computational Modeling

Ex-vivo intact, whole human atrial preparations (n=7), with a variety of comorbidities (**Tables S1** and **S2**), were mapped during pacing-induced sustained AF using a novel integrated approach involving high-resolution near-infrared optical mapping (NIOM, 0.33-0.9 mm^2 resolution) in all 7

ex-vivo hearts and simultaneous clinically-employed MEM (9 mm^2 resolution) in 6 hearts, as previously described.[11, 13, 20] Explanted hearts were cardioplegically-arrested and cooled to 4°C in the operating room, during transport, dissection, and cannulation. Intact human biatrial preparations were isolated, coronary-perfused and superfused with 36.5±0.5°C oxygenated Tyrode's solution under constantly maintained pH (7.35±0.05) and pressure (55±5 mmHg), immobilized with pre-warmed and filtered 10μM blebbistatin (Abcam), and stained with pre-warmed and filtered near-infrared voltage sensitive dye di-4-ANBDQBS (10-40μM, University of Connecticut).[11, 13, 20] Diazoxide was added to cardioplegic solution immediately following recovery of the heart from the donor, as well as during dissection to prevent cell swelling and edema in explanted human cardiac tissue.[48] Preparations were then equilibrated for 20 to 30 minutes before any recordings. All preparations excluded regions of poor coronary perfusion/ischemia consequently poorly perfused tissue was trimmed and arterial leaks were ligated with silk sutures. Trimmed areas were limited and located adjacent to the surgical cut, which never interfered with atrial arterial supply or the viability of tissue for optical mapping. Optical activation times for each pixel were marked at the maximum positive derivative of the optical action potential upstroke or using 50% of the OAP amplitude (AP50%). *Ex-vivo* AF cycle length (AFCL) presented as milliseconds calculated from driver dominant frequency obtained by Fast Fourier Transform.

As previously described,[11, 20] all atrial preparations underwent subsequent high-resolution gadolinium-based contrast-enhanced magnetic resonance imaging (CE-MRI) (9.4T, Bruker BioSpin Spectrometer, Ettlingen, Germany) to quantify fibrosis distribution at a spatial resolution of ~175μm^3. CE-MRI-detected fibrosis was defined as gadolinium-enhanced voxels with signal

intensity exceeding a certain threshold. *Ex-vivo* heart-specific CE-CMR fibrosis thresholds were validated by utilizing ImageJ to quantify the fibrosis content of 1-3 Masson's trichrome stained sections from right and left atria. Two blinded analyzers found fibrosis percentages for each slide, and the average histology fibrosis values for each region were used to validate the fibrosis percent for their corresponding 2D CE-CMR sections.

Three-dimensional (3D) CE-MRI of Heart 5 (170×170×297μm³) and Heart 4 (178x178x360μm³) were chosen as representative examples and were interpolated to isotropic ratios for computer modeling. Computer models included heart-specific atrial anatomy, 3D fibrosis distribution, myofiber orientation, and wall thickness. Fiber orientation was estimated using the structure tensor approach, and 3D wall thickness was estimated by solving the Laplace equation, as previously described.[20] NIOM and the 3D human atrial model were reconciled using atrial anatomical landmarks. NIOM activation maps of the reentrant driver and structural analysis of Heart #4 and Heart #5 have been published elsewhere[6, 13, 20], but this is the first presentation of biophysically accurate computer models based on these hearts.

The propagation of electrical activation in the realistic 3D human atrial geometry can be simulated by solving the cardiac monodomain equation using a voxel-based finite difference solver.[49, 50] In this study, the most established human atrial Courtemanche-Ramirez-Nattel (CRN) model[21] with chronic AF remodeling[22], which includes the most up-to-date measured human cellular data[51], was further adapted to recreate the optically-recorded regional action potential durations in the right atrial region of Heart #5 (**Figure S3** and **Table S5**). Conductivity (10:1 longitudinal vs latitudinal) was adjusted to reproduce Heart #4 conduction velocity and anisotropy near pacing location by using our previously published approach.[20] This experimentally-validated cellular model was then applied across both atria.[52, 53] Fibrosis was modeled as non-conducting tissue.[54, 55] AF was induced

in the model by gradually reducing stimuli intervals until arrhythmia was induced or conduction failed from 12 randomly selected sites in the right atrium or left atrium. Adenosine challenge was modeled by the addition of $I_{K(Ado)}$ currents[23] with twice the current in the right atrium vs the left atrium, based on our previous NIOM study.[13]

Persistent AF Patient Population

The study was approved by the Ohio State University Wexner Medical Center Institutional Review Board and the Committee on Quality and Safety. Adenosine bolus during AF ablation is standard-of-care and does not require separate consent. Ten patients between November 2016 and December 2018 at The Ohio State University Wexner Medical Center (**Table S7)**, undergoing first-time (n=3) or redo (n=7) ablation of persistent AF utilizing FIRMap basket-catheters were included in the current study, who experienced acute change in AF pattern due to limited ablation during the procedure, noted as acute termination to sinus rhythm, conversion to atrial tachycardia, or slowing of AF cycle length (AFCL) by ≥10% (**Table S8**). Four of these patients consented to delayed-enhancement cardiac magnetic resonance (DE-CMR) scans to quantify the amount and location of atrial fibrotic tissue prior to ablation and were enrolled in our parallel trial on AF structural substrate (NCT03444337).

***In-Vivo* Electrophysiology Study**

All patients had antiarrhythmic medication held 5 half-lives prior to the electrophysiology study except amiodarone, which was stopped 5 weeks prior to the study when feasible. Each patient underwent right and left femoral venous cannulation with three and two femoral venous sheaths respectively. Two sheaths were then sequentially replaced by two trans-septal sheaths after

systemic anticoagulation followed by trans-septal puncture. Electroanatomic mapping of the left atrium was pursued via a CARTO system (CARTOv4 in 3 patients and CARTOv6 in 7 patients) and pulmonary vein isolation (PVI) was established or re-established. In Patient 8, PVI was conducted after AF driver mapping and ablation. If the patient was in sinus rhythm, AF was induced with rapid overdrive pacing with cycle lengths down to 190ms, without the use of isoproterenol. Subsequent basket-catheter mapping was performed with FIRMap™ Catheters (50-60 mm, Abbott EP) and unipolar electrograms were recorded for 1 minute (Pruka, GE CardioLab). Adenosine (0.15-0.2mg/kg, from either 6mg or 60mg vials)[14] was injected by intravenous bolus at the onset of recording, such that the first 8-16s recorded baseline conditions prior to the adenosine effect (**Figure 5)**. The 1-minute recordings were then exported and run on RhythmView™ (Abbott EP) to create activation movies. Left atrial mapping was followed by targeted ablation at sites described below. If necessary, the right atrium subsequently underwent electroanatomic mapping with identification of phrenic nerve and His Bundle locations, the basket catheters were deployed, and the process above was repeated.

In-Vivo Activation Patterns guiding Targeted Ablation

Activation movies were assessed by the operator to identify possible sustaining mechanisms of AF. One-minute recordings were divided into 4s segments. The operator used all 4s segments within the 1-minute recordings to plan ablation, with emphasis on the two default segments chosen by RhythmView, currently a proprietary algorithm (Abbott EP). The operator considered both baseline and adenosine segments when identifying reentrant or focal driver patterns for targeted ablation, limited to a 1x1-2x1 inter-electrode distance at the portion of the driver activation pattern visualized with highest stability. A proprietary algorithm for defining possible rotation, Rotational

Activity Profile (RAP), mapped each 4s segment and was also considered by the operator when planning ablation, although targeted ablation was often adjacent to RAP locations. In 13/15 targeted ablations, initial lesion sets were connected by a linear lesion to an unexcitable anatomic obstacle such as the superior vena cava or PVI lesion. Arrhythmia pattern and AFCL were assessed after each ablation lesion set.

In-Vivo Driver Physiology Analysis

An AF driver was defined as any location where limited ablation caused acute termination to sinus rhythm, conversion to atrial tachycardia, or slowing of AFCL by ≥10%. All driver visualization and AFCL data were analyzed after offline, semi-automatic correction of RhythmView activation annotations based on $-dV/dt_{max}$ criteria of non-processed unipolar electrograms on a customized MatLab program. Then, visualization patterns were reassessed on RhythmView activation movies and presented as activation maps ($-dV/dt_{max}$) created with a customized MatLab program. Activation patterns at the driver site were categorized as either reentrant (>270° rotation), partial reentrant (>180° rotation), focal (centrifugal activation), or disordered throughout the 4s segments across the 1-minute recording (**Figure S5**). Temporal stability of activation patterns was quantified as the percent of total activations over the 4s segment.

Local AFCL was measured offline at every electrode during the 4s segments as the median time between atrial deflections. Driver AFCL was determined by the average of the median AFCL for 4-6 electrodes constituting the driver activation pattern at the termination site and was compared to all other non-driver electrodes. Electrogram stability is reported as the SD of local AFCLs over 4s (**Figure S4**).

In-Vivo Delayed-Enhancement Cardiac Magnetic Resonance Imaging

Patients 1, 7, 8, and 10 underwent DE-CMR scans using a 3T MAGNETOM Tim Trio (Siemens HealthCare) with a spatial resolution of 0.8854mm^3 (Patient 1) or 0.625x0.625x1.25mm^3 (Patients 7, 8, and 10), as previously described.[26] Patients 7, 8, and 10 did not have any prior ablations, while Patient 1 had prior ablations confined to the LA. Briefly, DE-CMR scans were acquired 18–25 minutes following injection of 0.2mmol/kg gadolinium agent. An electrocardiogram-gated, fat-suppressed 3D inversion recovery gradient recalled echo sequence with respiratory navigator gating was used. Typical scan parameters were as follows: echo time, 2ms; flip angle, 20°; inversion time, 300ms; repetition time, 4.4ms; and receiver bandwidth, 355Hz/pixel, 8–10min scan time. 3D image data covering the entire heart including both atria and ventricles were acquired and reformatted into 2D cross-sections. DE-CMR images were interpolated to an isotropic resolution, the atrial chamber walls were manually identified and segmented, and volume rendered as a 3D reconstruction using Amira software (FEI Company). An image intensity ratio was calculated by dividing the atrial wall intensity by blood pool intensity, with atrial fibrosis exceeding a patient-specific ratio (1.0-1.2) in accordance with previously published atrial fibrosis quantification studies using a similar method.[25, 26] A 1x1cm^2 region, spanning the thickness of the wall, at the driver site and the surrounding 1x1cm^2 regions composing a 3x3cm^2 grid were individually segmented and fibrosis content quantified. These 9 driver regions were compared to randomly selected 1x1cm^2 regions outside the driver region within the same atrial chamber for each patient.

Statistical Analysis

Data are presented as mean ± standard deviation unless otherwise stated in figure legends. Analysis was done in R 3.4.4 using packages lme4 and emmeans. Measurements were taken from distinct samples. Baseline values recorded from the same patient or *ex-vivo* heart were used as the control values when comparing the effect of adenosine. Statistical analysis was done using a general linear model with heart/patient as a factor to control for multiple drivers being observed in the same heart or patient. The mixed models used in analysis of AFCL data included median measurements over 4s as a Response and Condition, Driver Category, Patient, Adenosine Dose, and Atrium as predictors. Patient was treated as random effect, all other predictors as fixed effects. The mixed models used in analysis of fibrosis data included Fibrosis Percentage as response and Driver Category and Patient as predictors. Patient was treated as random effect and Driver Category as fixed effect. Observations were weighted by inverse of standard deviations for each Patient, Atrium and Driver Category combination to mitigate unequal sample sizes. Logistic regression with adenosine-improved or adenosine-obscured as a response and Baseline values in reentrant driver visualization stability as predictor was used to select the optimal threshold corresponding to maximal accuracy of predicting improvement in driver stability by adenosine. Pairwise comparisons were done with Tukey adjustment. P-values <0.05 were considered significant. Modeling assumptions were monitored by visual inspection of residuals.

In order to determine a correlation between baseline AFCL and change in AFCL (Delta) induced by adenosine challenge, the robust model was fitted using the robustlmm package in R. The Delta was used as a response and ID and Baseline values as predictors. The ID, the unique combination of Patient and Driver IDs, was treated as random effect, and Baseline values as continuous covariate. The confidence intervals for model coefficients were estimated via bootstrapping using R package boot with 500 replicates.

The statistical power and sample size calculations for post-hoc (achieved power) and a priori (prospective studies) were done with G-power 3.1.9.2 (University of Dusseldorf) using F-test option at the 95% confidence level. The minimal adequate statistical power was assumed at 80% level. The achieved statistical power was calculated for the effect sizes estimated as the ratio of variance explained by the adenosine effect to the residual variance. The variances were estimated based on mixed models fitted using R package lme4. The Treatment group was modeled as a fixed effect and Driver ID nested within Heart ID as a random effect to properly account for multiple drivers present in some hearts. The variances were extracted using R package insight.

The highest f1-score was used to determine best predictive thresholds. f1-score was calculated as the harmonic mean of precision and recall, see formula below.

f1-score = $(2 \cdot \text{precision} \cdot \text{recall})/(\text{precision} + \text{recall})$.

SUPPLEMENTAL TABLES

Table S1. *Ex-Vivo* Human Heart Histories

Heart No.	Age	Sex	Prep	Heart Weight	Diagnoses
Heart #1	54	M	Intact	720	AF, HF, HTN, Diabetes
Heart #2	61	M	Intact	589	AF, HF, AVN ablation and BiV pacemaker, OSA, HLD
Heart #3	61	M	Intact	480	AF, HF, ICD, CAD, OSA, Pacemaker, VT
Heart #4 [20, 56]	63	F	Intact	608	HTN, Hypothyroidism, AF seen at time of explant
Heart #5 [6, 13]	54	M	Intact	474	HTN, HLD
Heart #6	33	M	Intact	650	Multi-substance Abuse
Heart #7	58	M	Intact	462	HTN

Previous references in which some hearts were included shown in parentheses. AF-atrial fibrillation; AVN-atrioventricular node; BiV-biventricular; CAD-coronary artery disease; HF-heart failure; HLD-hyperlipidemia; HTN-hypertension; ICD-implantable cardioverter-defibrillator; LVAD-left ventricular assist device; NICM-non-ischemic cardiomyopathy; OSA-obstructive sleep apnea; VT-ventricular tachycardia.

Table S2. *Ex-Vivo* Human Heart Protocols

							Improved by Adenosine	
Heart No.	**CE-MRI**	**Simulation**	**MEM**	**Driver**	**Ablation**	**Adenosine**	**NIOM**	**MEM**
Heart #1	Yes	No	Yes	1	Yes	Injection	Yes	Yes
				2	Yes		Yes	No
Heart #2	Yes	No	Yes	1	Yes	Injection	Yes	Yes
				2	Yes		No	Yes
Heart #3	Yes	No	Yes	1	Yes	Injection	Yes	Yes
Heart #4	Yes	Yes	No	1	No	N/A	N/A	N/A
				2	No		N/A	N/A
				3	No		N/A	N/A
Heart #5	Yes	Yes	Yes	1	No	Perfusion	Yes	Yes
				2	No		N/A	N/A
Heart #6	Yes	No	No	1	No	Injection	Yes	N/A
				2	No		No	N/A
Heart #7	Yes	No	No	1	No	Injection	No	N/A

CE-MRI-contrast-enhanced magnetic resonance imaging; MEM-multi-electrode mapping; NIOM-near infrared optical mapping.

Table S3. Experimental Duration

	Sustained AF condition
Case No.	**Pharmacological stimulation**
Heart #1	None
Heart #2	Iso 10nM+Pina 10μM
Heart #3	Iso 10nM+Pina 10μM
Heart #4	Iso 10nM
Heart #5	None
Heart #6	Iso 1nM
Heart #7	Iso 10nM

Ado-adenosine; Iso-isoproterenol; Pina-pinacidil.

Table S4. Effect of Adenosine on *Ex-Vivo* Human Hearts

Case No.	Driver	Group	Baseline % Temporal Stability	Adenosine % Temporal Stability	Baseline AF CL (ms)	Adenosine AF CL (ms)	Driver Location	AF CL % Delta
Heart #5	1	Improve	76	95	152	72	Right	53
Heart #6	1	Improve	57	81	159	78	Right	51
	2	Obscure	100	0	171	142	Left	17
Heart #1	1	Improve	19	30	250	145	Right	64
	2	Improve	25	56	250	90	Right	42
Heart #2	1	Obscure	72	53	139	179	Right	-29
	2	Improve	20	32	139	179	Right	-29
Heart #3	1	Improve	33	75	125	114	Right	8
Heart #7	1	Obscure	60	0	116	95	Left	18
Avg ± SD		Improve	38± 23	62± 27	179± 56	113± 42	Right	23± 39
		Obscure	77± 21	18± 31	142± 28	139± 42	Left	18± 0.7

AF CL-atrial fibrillation cycle length; Avg- average; SD- standard deviation;

Table S5. Cellular model adapted to optical mapping values

Current	Current conductivity (nS/pF)
g_Na	7.8
g_K1	0.18
g_to	0.05782
g_Kr	0.0294
g_Ks	0.258
g_CaL	0.19808
g_bCa	0.00113
g_bNa	0.000674
g_IKACh	0.135
g_Kur	Voltage dependent, halved from original CRN
I_NaCa_max	2560 (pA/pF)
I_NaK_max	0.6 (pA/pF)
I_up_max	0.0075 (mM/ms)
C_m	120 (pF)

Cellular model based the previous published Courtemanche, Ramirez and Nattel(14) that was adapted to replicate chronic atrial fibrillation.(15)

Table S6. 3D Computational Simulation of Heart #5

	Fibrosis 70%	**Fibrosis 100%**	**Fibrosis 130%**
Adenosine 0%	Non-inducible	Unstable reentry for ~400 ms, CL ~132 ms	Unstable reentry for ~280 ms, CL ~137 ms
Adenosine 50%		Non-inducible	
Adenosine 100%	Non-inducible	Stable reentry throughout simulation, CL ~100 ms	Non-inducible
Adenosine 200%	Non-inducible	Stable reentry throughout simulation, CL ~96 ms	Non-inducible

CL-Cycle Length

Table S7. Persistent Atrial Fibrillation Patients' Demographics

Patient Info (n=10)	Average	Min	Max
Age (years)	61	49	75
Sex	30% Female		
Years Since AF diagnosis	5.6	1	11
Prior Ablations	0.8	0	2
CHADS2VASc Score	2.6	0	5
LA Dilation	40% Normal	40% Mild	20% Moderate
RA Dilation	80% Normal	20% Mild	
LV Ejection Fraction (%)	61	55	69
Heart Failure	30%		
Hypertension	80%		
Diabetes	30%		
Coronary Artery Disease	20%		
Obstructive Sleep Apnea	70%		
Body Mass Index	33	20	46
Presenting in AF	20%		
Previously intact PVI	30%		
Total RFA (minutes)	37.9	11.5	80.1
DE-CMR	40%		

AF-atrial fibrillation; DE-CMR-delayed-enhancement cardiac magnetic resonance; LA/RA-left/right atrium; LV-left ventricle; PVI-pulmonary vein isolation.

Table S8. Acute Outcomes of Driver ablation in Persistent Atrial Fibrillation Patients

Patient	1st Driver Outcome	2nd Driver Outcome	3rd Driver Outcome
1	Acute Termination (A-I)		
2	Acute Termination (A-I)		
3	Acute Termination (A-I)		
4	Conversion to AFL (A-I)		
5	Acute Termination (A-O)	Acute Termination (A-O)	
6	Acute Termination (A-I)	Acute Termination (A-O)	
7	Slowed (17%) (A-O)	Slowed (11%) (A-O)	Conversion to AFL (A-O)
8	Acute Termination (A-O)		
9	Acute Termination (A-I)	Acute Termination (A-I)	
10	Conversion to AFL (A-I)		

If 1st Driver was acutely terminated, 2nd Driver, if present, was mapped and ablated after AF reinduction. AFL- atrial flutter; A-I adenosine-improved; A-O adenosine-obscured.

Table S9. Long-term Follow-up of Patients

Patient	# of Drivers	PVs found reconnected	12 month rhythm	Anti-arrhythmic drugs at follow-up
1	1	0	AT	diltiazem
2	1	2	SR	diltiazem/ dofetilide
3	1	0	SR	metoprolol
4	1	0	SR	metoprolol
5	2	2	SR	sotalol
6	2	2	SR	metoprolol
7	3	First PVI	AF	sotalol
8	1	First PVI	SR	metoprolol
9	2	3	SR	dofetilide
10	1	First PVI	AF	carvedilol

AF-atrial fibrillation; AT-atrial tachycardia; PV(I)-pulmonary veins (isolation); SR-sinus rhythm

SUPPLEMENTAL FIGURES

Figure S1. Experimental Procedure Flowchart

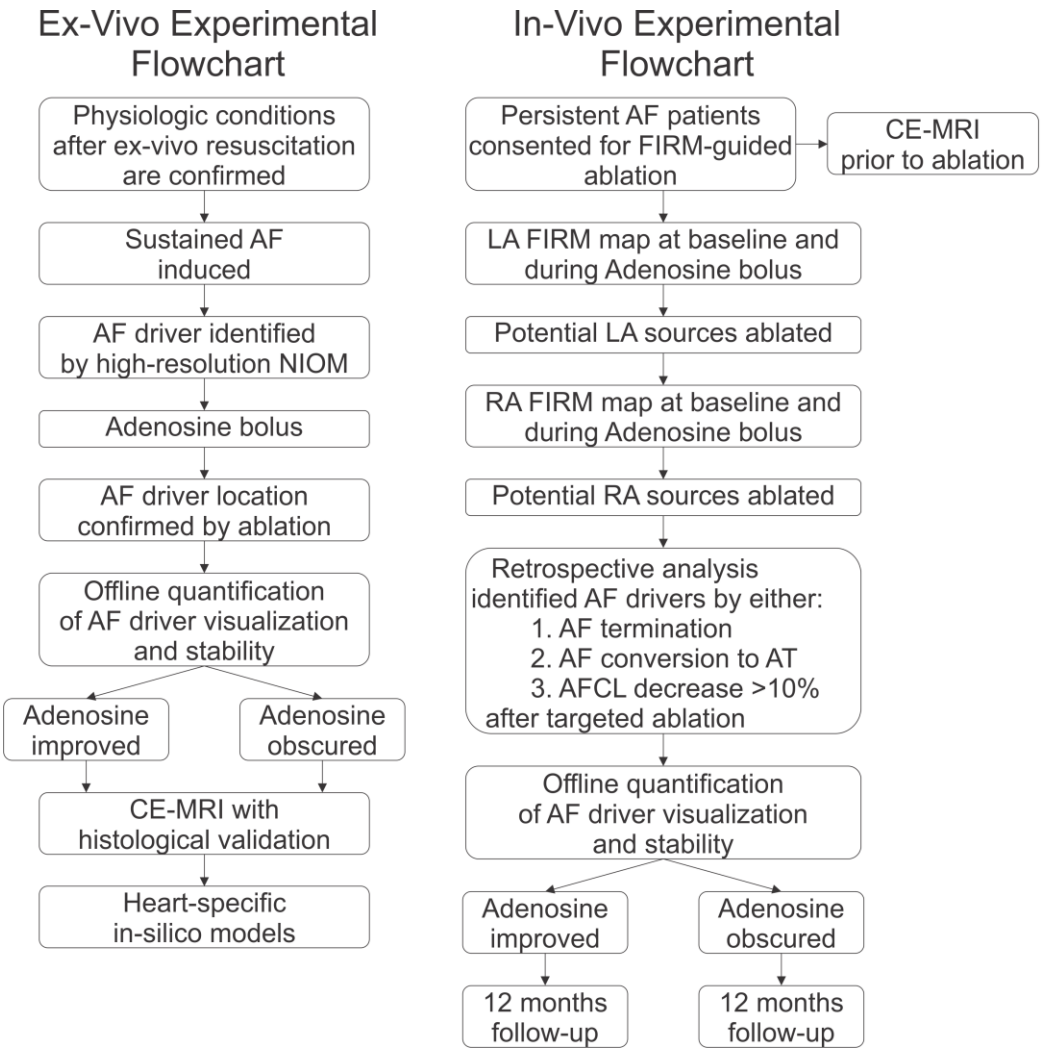

Left, Experimental procedure flowchart for the study of adenosine-induced changes in atrial fibrillation (AF) driver visualization in ex-vivo human hearts by near infrared optical mapping (NIOM). Right, Experimental procedure flowchart for the study of adenosine-induced changes in AF driver visualization in persistent AF patients. AFCL-atrial fibrillation cycle length; AT- atrial tachycardia; CE-MRI-contrast enhanced magnetic resonance imaging; FIRM-focal Impulse and Rotor Mapping; LA/RA-left/right atrium.

Figure S2. Validation of CE-CMR by histology sections

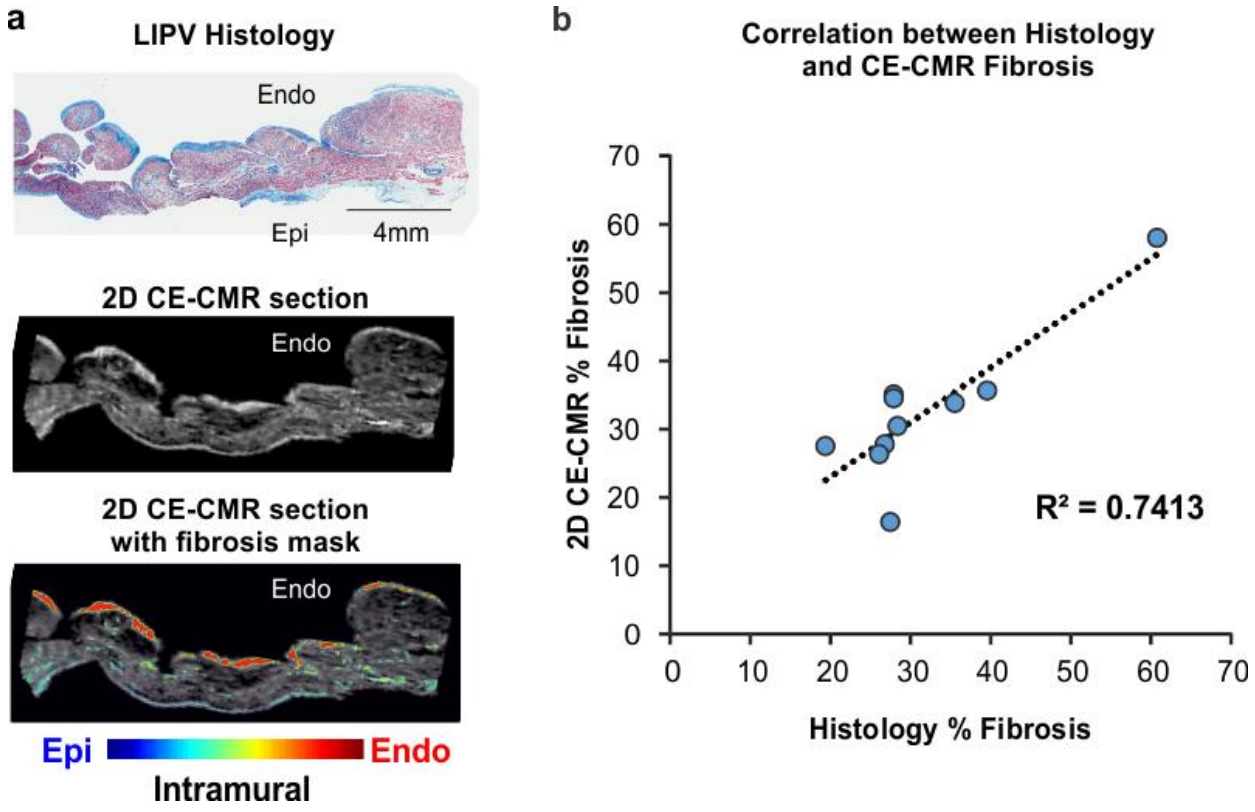

a, Top to bottom: Masson's trichrome stained section of the left inferior pulmonary vein (LIPV) showing fibrosis in blue and myocytes in red. Co-registered two-dimensional (2D) section from the high-resolution (100µm^3) *ex-vivo* contrast-enhanced cardiac magnetic resonance (CE-CMR) imaging. The same 2D section as above with fibrosis shown colored by transmural location with signal intensity threshold validated to have a comparable percent of fibrosis as histology. **b,** Graph showing correlation between histology section fibrosis and 2D CE-CMR fibrosis for all studied *ex-vivo* heart. Endo-endocardium; Epi-epicardium.

Figure S3. Activation patterns during pacing in heart-specific 3D computational human atrial model of Heart #5

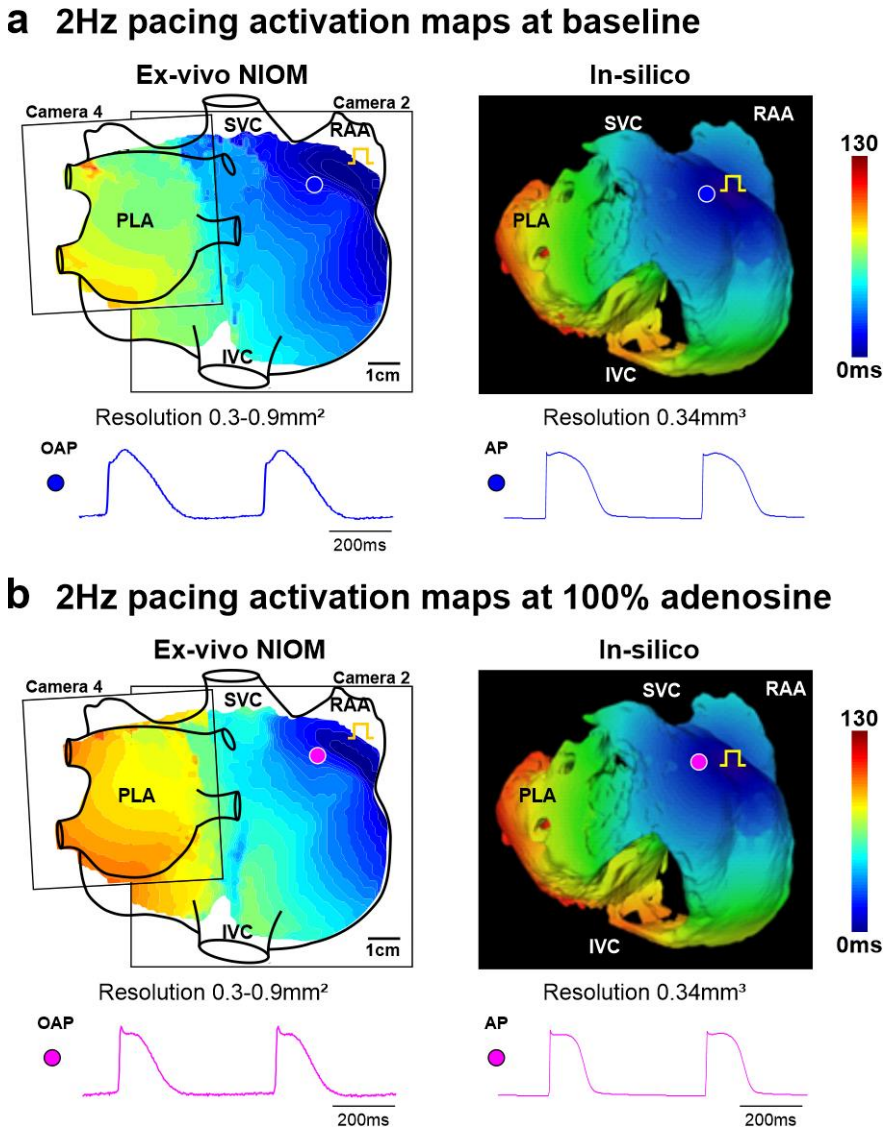

Near-infrared optical mapping (NIOM) and 3D heart-specific model activation maps and representative optical/simulated action potentials during 2Hz pacing during baseline (**a**) and 100% adenosine (**b**) conditions. Square pulse symbol represents pacing location. I/SVC-inferior/superior vena cava; OAP/AP-optical/action potential; PLA-posterior left atrium; RAA-right atrial appendage.

Figure S4. Time-dependent AF reentrant driver visualization and cycle length changes during adenosine challenge.

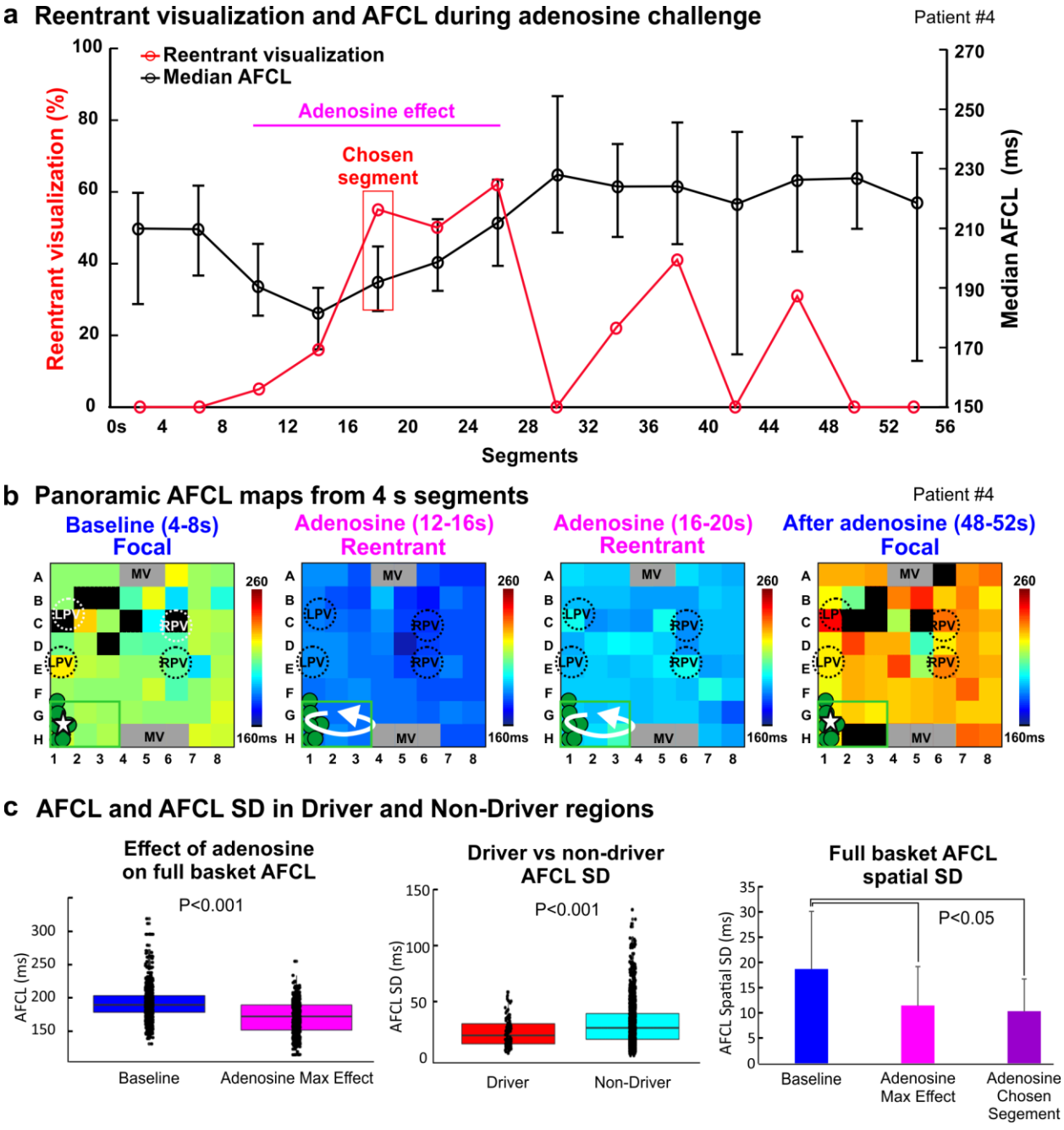

a, Full-basket median atrial fibrillation cycle length (AFCL) and reentrant visualization of the atrial fibrillation (AF) driver for each 4s segment in Patient #4. Error bars on median AFCL graph show interquartile range. **b**, representative full-basket median AFCL maps from Patient #4. Green circles indicate AF terminating ablation lesions. **c,** Box plots demonstrating the effect of adenosine on AFCL and AFCL SD in driver and non-driver regions. **Left,** Box plot of full-basket median atrial fibrillation cycle length (AFCL) at baseline and during adenosine. Statistical analysis compared to baseline was done using a general linear model. **Middle,** Box plot of beat-to-beat AFCL standard deviation (SD) from electrodes in the AF driver region and all non-driver electrodes. Statistical analysis compared to driver was done using a general linear model. **Right**, Bar graph comparing the SD of AFCL between all basket electrodes not overlying atrioventricular valves or in poor contact during the average of baseline segments, the segment with the maximum adenosine effect, and the adenosine segment with highest driver visualization. Statistical analysis compared to baseline was done using a general linear model. MV-mitral valve; LPV-left pulmonary veins; RPV-right pulmonary veins.

Figure S5. Variable driver visualization patterns seem by multi-electrode mapping in persistent AF patients.

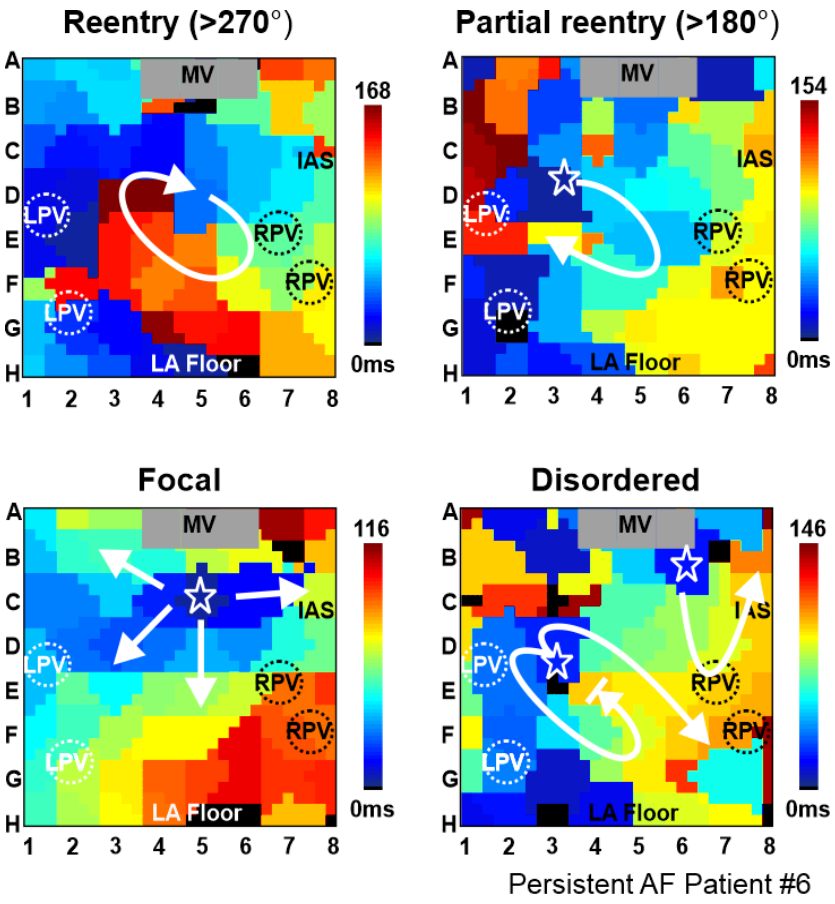

AF Driver visualization patterns were classified as reentrant (>270° rotation), partial reentrant (>180° rotation), focal (centrifugal activation), or disordered. MV-mitral valve; LPV-left pulmonary veins; RPV-right pulmonary veins; IAS-interatrial septum; LA-left atrium.

Figure S6. Low-resolution mapping overestimates reentrant driver path

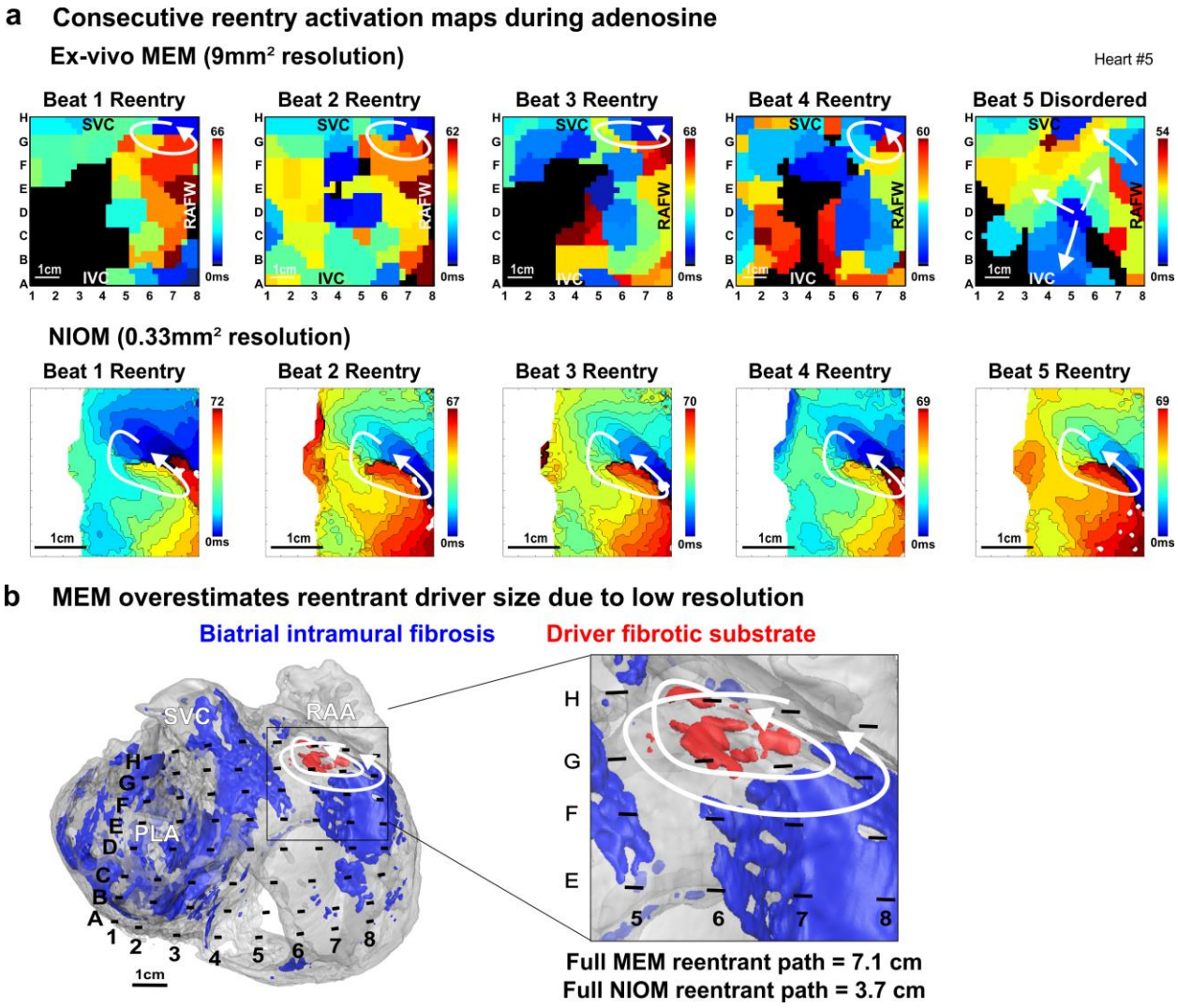

a, Five consecutive activation maps showing activation patterns recorded simultaneously from multi-electrode mapping (MEM) (**Top**) and near-infrared optical mapping (NIOM) (**Bottom**) of *ex-vivo* human atria at the same driver location. **b,** Intramural fibrosis in the atrial fibrillation (AF) driver region (red) and within the surrounding 3D human atrial structure (blue) seen by contrast-enhanced magnetic resonance imaging (CE-MRI) with overlapped MEM array. SVC-superior vena cava; PLA-posterior left atrium; RAA-right atrial appendage; RAFW-right atrial free wall.

Figure S7. Limited ablation lesions necessary to terminate AF in Heart #1

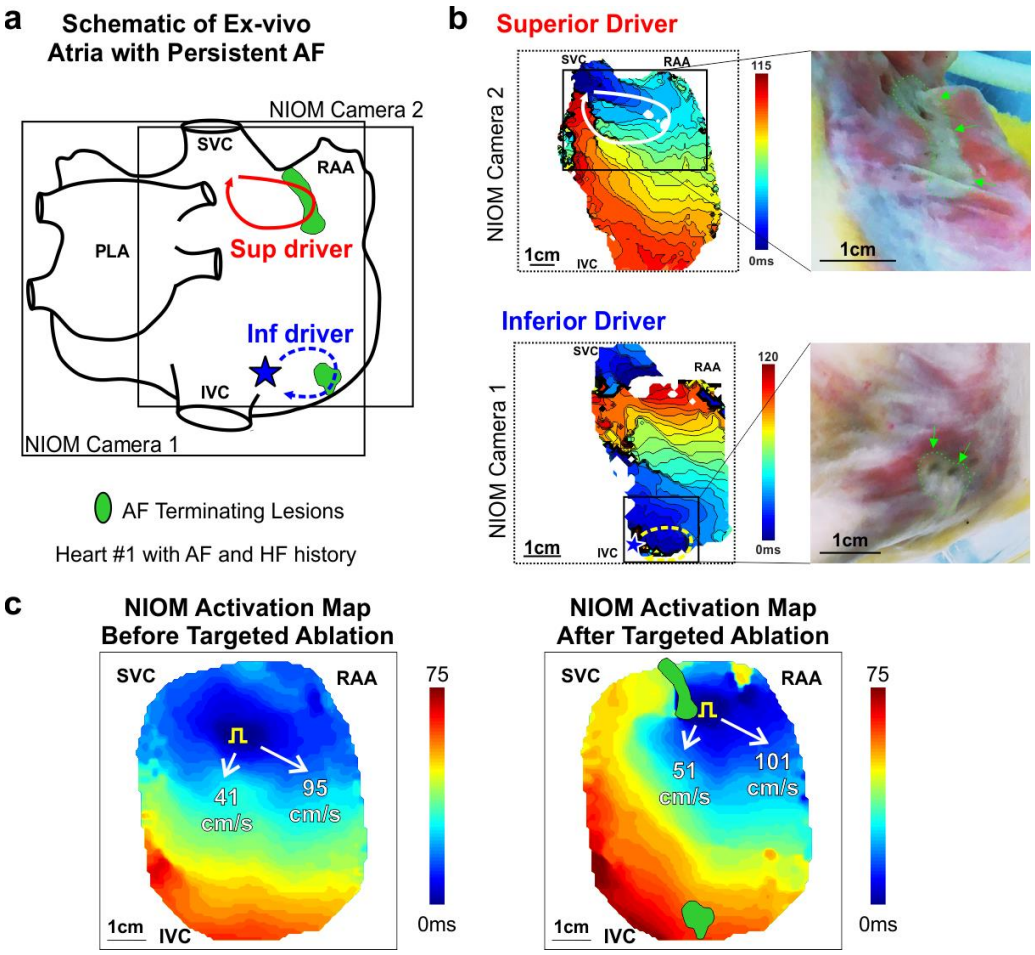

a, Schematic of the human atrial preparation showing locations of the two competing atrial fibrillation (AF) drivers and the ablation lesions (green) that terminated them and prevented the reinduction of AF. **b,** Near-infrared optical mapping (NIOM) action maps for the superior (Sup, **top**) and inferior (Inf, **bottom**) reentrant AF drivers with photos of the ablation lesions (marked with green arrows) shown to the right. **c,** NIOM activation maps at 500ms cycle length pacing just prior to AF induction (**left**) and after AF termination by ablation (**right**). Optical field of view in right panel moved down and to the left 5mm. Square pulse symbol represents pacing location.

MV-mitral valve; PLA-posterior left atrium; RAA-right atrial appendage; I/SVC-inferior/superior vena cava; HF-heart failure.

Figure S8. Heart-specific 3D computational simulations of a baseline stable reentrant driver destabilized by adenosine challenge.

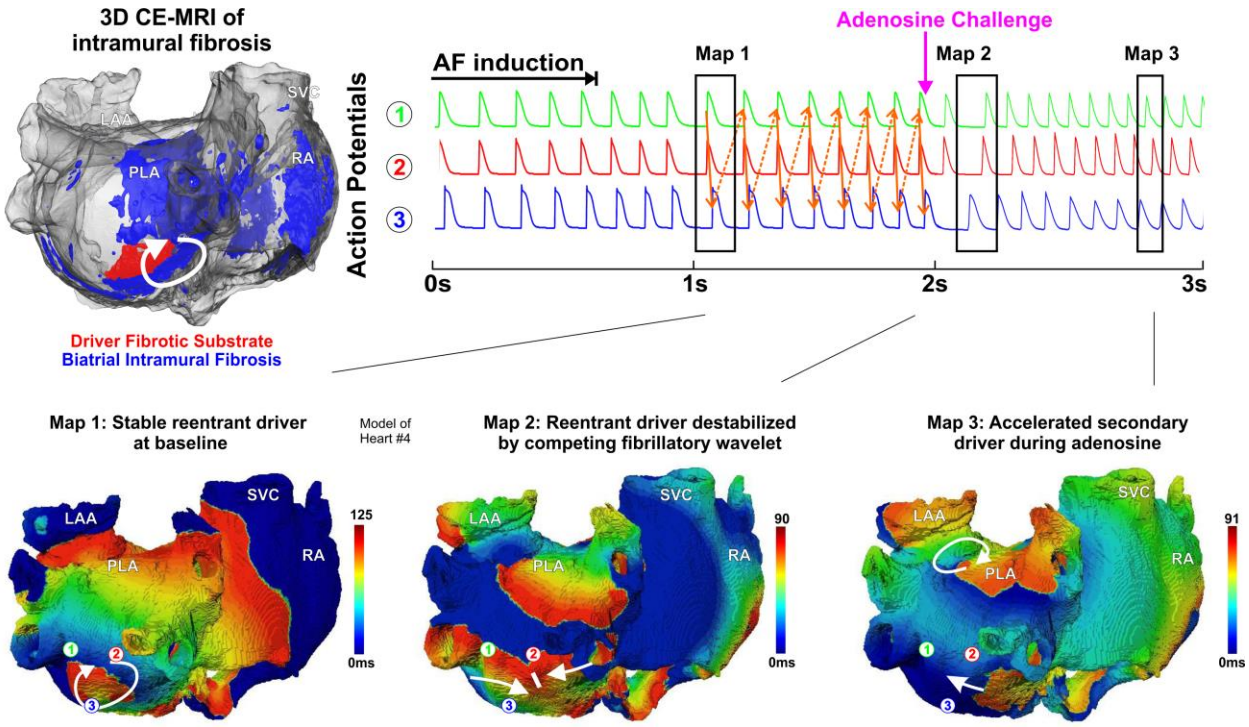

Top Left, 3D human atrial structure showing intramural fibrosis in the atrial fibrillation (AF) driver arrhythmogenic hub (red) and surrounding intramural fibrosis (blue) seen by contrast-enhanced cardiac magnetic resonance (CE-MRI) in Heart #4. **Top Right,** representative action potentials from the driver region. **Bottom Left to Right**, activation map showing a stable reentrant driver in the inferior posterior left atrium (PLA) during baseline AF. After adenosine is added to the model, an accelerated fibrillatory wavelet from the superior posterior left atrium (PLA) entered the widened excitable gap and collided with the reentrant driver. During adenosine, AF was maintained by an accelerated secondary, temporally-unstable driver. PLA-posterior left atrium; SVC-superior vena cava; LAA-left atrial appendage; RA-right atrium.

Figure S9. Reentrant driver NIOM activation maps for Figure 3

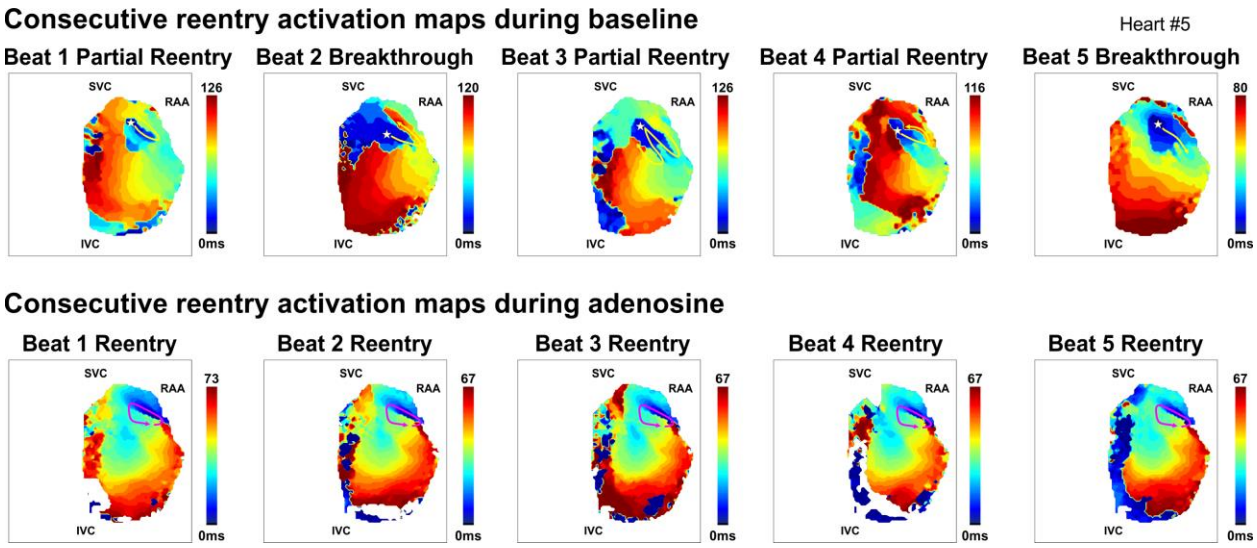

Top, Five consecutive near-infrared optical mapping (NIOM) activation maps of atrial fibrillation (AF) induced at baseline conditions show unstable, partial reentrant driver patterns from an intramural reentrant driver. **Bottom,** Five consecutive NIOM activation maps of AF induced during adenosine perfusion show adenosine stabilized the complete reentry pattern of the intramural reentrant driver at the atrial surface. RAA-right atrial appendage; I/SVC-inferior/superior vena cava.

Figure S10. Altering the relationship between fibrotic driver substrate and atrial refractoriness in 3D computational simulations of Heart #5

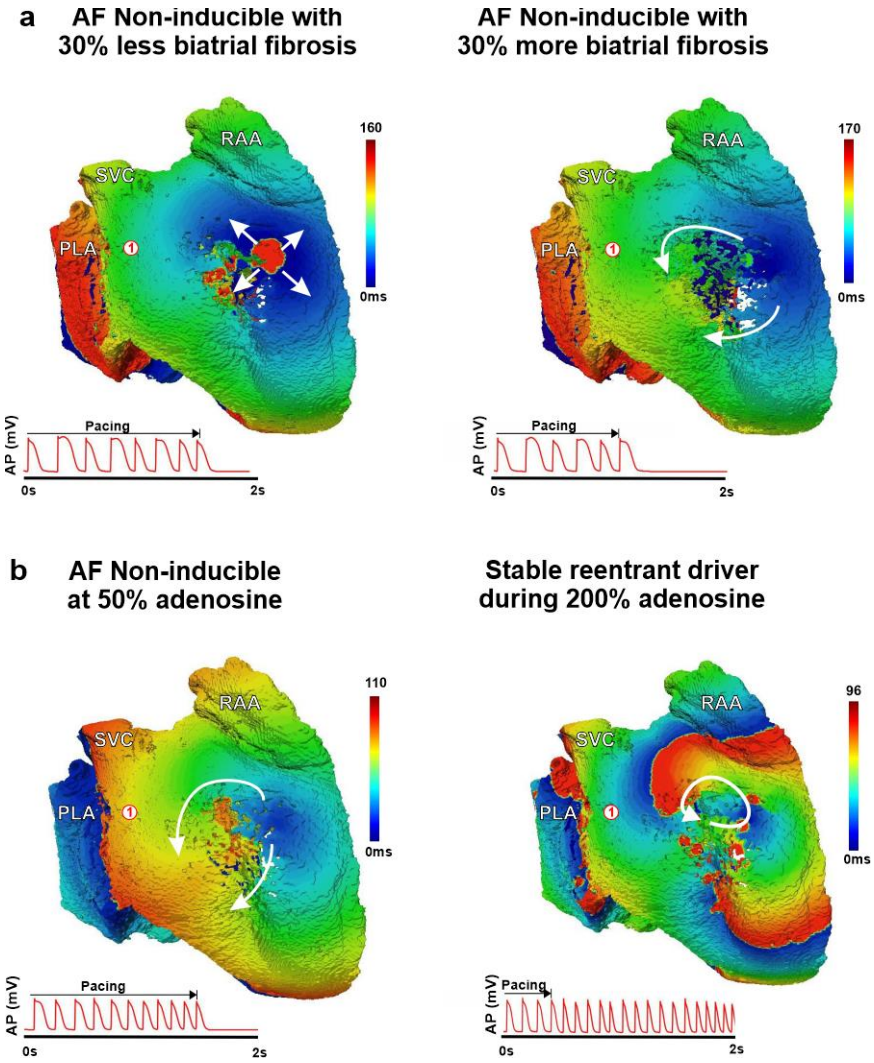

a, Adjusting the amount of biatrial fibrosis to 30% more or 30% less than that measured in the *ex-vivo* heart renders atrial fibrillation (AF) not inducible. **b,** Adjusting the amount of adenosine dosage to 50% or 200% renders AF not inducible or indictable, respectively. RAA-right atrial appendage; SVC-superior vena cava; PLA-posterior left atrium; AP-action potential.

Figure S11. Initial baseline stability predicts patient-specific response in driver visualization patterns during adenosine challenge

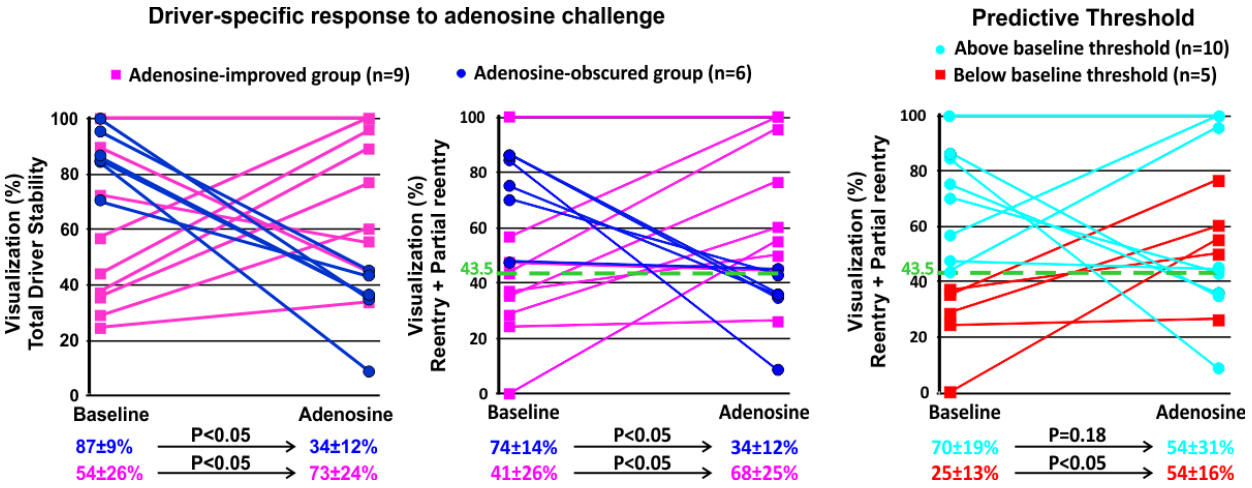

Left, Plots comparing total (left) and reentrant (middle) driver visualization stability between the adenosine-improved and adenosine-obscured groups. Statistics performed with a general linear model. **Right**, Logistic regression analysis of initial reentry visualization stability found a threshold of 43.5% (green dotted line) predicted significant improvement by adenosine with sensitivity 89% and specificity 83%. Statistical analysis compared to baseline was done using t-test.

SUPPLEMENTAL VIDEOS

Video S1. Near-infrared optical mapping (NIOM) activation movie of a sub-epicardial recording during baseline AF in intact atria, Heart #5. This AF visualization is also shown in **Figure 1**. Optical action potentials are shown below driver region, and locations are marked on the map by asterisks. IVC-inferior vena cava; RAA-right atrial appendage; SVC-superior vena cava.

Videos S2 and S3. Multi-Electrode Mapping (MEM) activation movies from an epicardial custom-flattened multi-electrode catheter recording during baseline AF in intact atria, Heart #5. Yellow arrows in **Video S3** show location and pattern of a partial reentrant driver as seen by NIOM. This AF visualization is also shown in **Figure 1.**

Video S4. NIOM activation movie of a sub-epicardial recording during AF under adenosine effect in intact atria, Heart #5. This AF visualization is also shown in **Figure 1**. Optical action potentials are shown below driver region, and locations are marked on the map by asterisks. IVC-inferior vena cava; RAA-right atrial appendage; SVC-superior vena cava.

Videos S5 and S6. MEM activation movies of an epicardial custom-flattened multi-electrode catheter recording during AF under adenosine effect in intact atria, Heart #5. Pink arrows in **Video S5** show location and pattern of a reentrant driver as seen by NIOM. This AF visualization is also shown in **Figure 1.**

Videos S7 and S8. MEM activation movie of an endocardial multi-electrode basket catheter recording during baseline AF in Patient #6. Ablation-confirmed driver located at electrodes DE45. Yellow arrows in **Video S7** represent common activation path of reentrant AF driver over five beats as shown in **Figure 6**.

Videos S9 and S10. MEM activation movies of an endocardial multi-electrode basket catheter recording of AF during adenosine bolus effect in Patient #6. Ablation-confirmed driver located at electrodes DE45. Pink arrow in **Video S9** denotes reentrant AF driver pattern as shown in **Figure 6**.

Video S11. MEM activation movie of an endocardial multi-electrode basket catheter recording during baseline AF in Patient #6. This AF visualization is also shown in **Videos S7** and **S8**, and **Figure 6**. Ablation-confirmed driver located at electrodes DE45 (green dots). Yellow arrows represent common activation path of reentrant AF driver over five beats at baseline and pink arrow represents consistent reentrant activation pattern of the same driver unmasked during adenosine challenge as in **Videos S9** and S**10**.